Journal of Solid State Chemistry 188 (2012) 17–25

Contents lists available at SciVerse ScienceDirect

Journal of Solid State Chemistry

journal homepage: www.elsevier.com/locate/jssc

Single crystalline and rare earth substituted La_2RuO_5 investigated by x-ray diffraction and EXAFS spectroscopy

S. Riegg [a,*], A. Reller [b], S.G. Ebbinghaus [c]

[a] Experimental Physics V, Center for Electronic Correlations and Magnetism, University of Augsburg, D - 86135 Augsburg, Germany
[b] Resource Strategy, University of Augsburg, D - 86135 Augsburg, Germany
[c] Solid State Chemistry, Martin-Luther University Halle-Wittenberg, D - 06099 Halle, Germany

ARTICLE INFO

Article history:
Received 8 September 2011
Received in revised form
22 January 2012
Accepted 26 January 2012
Available online 3 February 2012

Keywords:
La_2RuO_5
Rare earth substitution
Ruthenate
Layered perovskite
Single crystal structure analysis
EXAFS

ABSTRACT

Single crystals of La_2RuO_5 were obtained from a $BaCl_2$ flux. The structure was determined by single crystal x-ray diffraction and compared to earlier x-ray and neutron powder diffraction results. The local structures of Ru and La/*Ln* in pure La_2RuO_5 and the rare earth substituted $La_{2-x}Ln_xRuO_5$ (*Ln*=Pr, Nd, Sm, Gd, Dy) polycrystalline samples were determined from the extended x-ray absorption fine structures (EXAFS) of the K- and L_{III}-edges of Ru, La, and *Ln*, respectively. A four shell model was developed to reduce the number of refinable parameters in the fit of the EXAFS spectra. The distribution of the *Ln*-ions in the layered crystal structure was determined by a comparison of the coordination spheres obtained from the *Ln*-edges with the unsubstituted La_2RuO_5. Interatomic distances were compared to the values obtained from the single crystal diffraction and were found to agree very well.

1. Introduction

La_2RuO_5 shows a combined structural and magnetic phase transition at roughly 170 K [1–3]. Above this temperature the crystal structure is monoclinic (SG: $P2_1/c$) and a paramagnetic behavior of the Ru^{4+} ions is found. In addition La_2RuO_5 is semiconducting with a small bandgap of 0.15 eV. Below the transition temperature the change to triclinic symmetry (SG: $P\bar{1}$) is linked to an antiferromagnetic coupling of the $S=1$ spin moments of Ru^{4+} resulting in a local dimerization of neighboring Ru spins [4,5]. This ordering causes an almost complete suppression of the paramagnetic susceptibility. The low temperature modification is found to be still a semiconductor, but with an increased bandgap of 0.21 eV.

Single crystal structure data were not available to date, although the electrical conductivity of single crystals was reported in the literature [2]. From the crystal structure obtained by powder neutron diffraction [6], La_2RuO_5 can be described by a stacking of perovskite-like $LaRuO_4$- and LaO-layers, alternating along the unit cell axis **a**. This layering in combination with the small temperature range, in which La_2RuO_5 is formed (1150–1200 °C), is a problem for the growth of single crystals, which generally are twinned. Crystal growth by the floating zone technique has been reported [7], but our own attempts were not successful. Therefore, the single crystals described in this study were grown using $BaCl_2$ as a flux. Only twinned crystals were obtained, but the different domains could be refined separately in the crystal structure analysis.

To gain more information on the relationship of the structural and magnetic phase transition, La was partly substituted by smaller rare earths (Pr, Nd, Sm, Gd, Dy) [8,9]. The maximum achievable substitution level is depending on the difference of the ionic radii of Ln^{3+} compared to La^{3+}. Thus for Pr $x=0.75$ was achieved, while for Dy the maximum was reached at $x=0.2$. Above these values significant amounts of secondary phases were detected. The synthesis was carried out with a citrate based soft chemistry approach and lead to single phase polycrystalline samples. The magnetic properties of the rare earth substituted samples can be described assuming two almost independent magnetic sublattices. One sublattice consists of the above mentioned antiferromagnetically interacting Ru^{4+} ions, while the second sublattice is formed by the paramagnetic rare earth ions. This model was partly deduced from the distribution of the rare earth ions on the two possible crystallographic sites in La_2RuO_5. Neutron diffraction results for two Pr substituted powder samples ($La_{1.75}Pr_{0.25}RuO_5$ and $La_{1.25}Pr_{0.75}RuO_5$) revealed a cationic ordering with roughly 65–70% of the Pr ions in the LaO layers [9]. Due to very similar neutron scattering lengths and/or

* Corresponding author.
E-mail address: stefan.riegg@physik.uni-augsburg.de (S. Riegg).

0022-4596/$ - see front matter © 2012 Elsevier Inc. All rights reserved.
doi:10.1016/j.jssc.2012.01.057

huge absorption cross sections for Nd, Sm, Gd and Dy neutron diffraction was not applicable for the determination of the rare earth distribution. Therefore, a different method had to be used to investigate the localization of the rare earths in $La_{2-x}Ln_xRuO_5$.

EXAFS is a well established method to study the local crystal structure and the valence of a selected element [10]. Since EXAFS is highly element specific, in many cases even directly neighboring elements in the periodic table can be investigated separately. While the Ru environment in La_2RuO_5 already was object of investigations [11] and the Ru $L_{III,II}$-edges were used for the determination of the crystal field splitting of the Ru 4d levels [7], this was not the case for $La_{2-x}Ln_xRuO_5$, neither was the lanthanide local structure studied yet. According to the complex local environment of the two La/*Ln* sites a simplified model was developed to interpret the obtained EXAFS spectra. With this model the investigation of the site distribution of the substituted lanthanides became possible.

Additionally, in this work the single crystal structure results are compared with the already published powder data and with the values obtained from fitting the EXAFS spectra.

2. Sample preparation and experimental details

2.1. La_2RuO_5 single crystal growth and x-ray diffraction

Single crystals of La_2RuO_5 were obtained by a flux assisted method. The dried (6 h at 850 °C) binary oxides La_2O_3 (Chempur, 99.9%) and RuO_2 (Chempur, 99.9%) were weighed in stoichiometric amounts (0.5325 g of La_2O_3 and 0.2175 g of RuO_2), mixed and well ground in an agate mortar. This powder was mixed with 6.25 g $BaCl_2$, which was dried at 120 °C. The mixture was reacted in uncovered aluminum-oxide crucibles in a tube furnace by heating to 1200 °C in 4 h, holding this temperature for 6 h and slow cooling to 950 °C with a rate of 3 K/h to get below the melting temperature of $BaCl_2$. At this temperature the furnace was switched off and allowed to cool down to room temperature. The excess $BaCl_2$ was dissolved in deionised water. In the crucible La_2RuO_5 and LaOCl [12] remained, which had to be removed manually. The black La_2RuO_5 crystals were separated from the colorless LaOCl crystals under a microscope. The obtained single crystals had a plate-like form with a size of roughly $0.05 \times 0.05\ mm^2$ and a thickness of less than 30 μm. This shape results from the layered structure, which also causes the observed twinning of the crystals.

From the obtained crystals an almost square shaped individual was selected. A STOE IPDS 2T single crystal diffractometer operating with $Mo-K_\alpha$ radiation was used to record the reflections in the angular range $5^\circ \le 2\theta \le 80^\circ$. The numerical absorption correction was carried out using the measured crystal shape and size obtained from the indexing of the visible surfaces. This shape was optimized using the HABITUS type approach [13] implemented in the X-Shape algorithm of the STOE data reduction software package. Further information about the measurement parameters are listed in Table 1. The absorption corrected intensities were refined with SHELX starting from the structural information determined from the powder data [14].

2.2. $La_{2-x}Ln_xRuO_5$ powder sample preparation and EXAFS

Powder samples of $La_{2-x}Ln_xRuO_5$ were prepared by a citrate based sol gel reaction described in more detail elsewhere [9]. Starting materials were the rare earth nitrates, Ru-acetylacetonate and citric acid, which were dissolved in ethanol (96%). The precursors were pyrolysed at 600 °C and finally calcined for at least 96 h at 1175 °C in alumina crucibles in air. Phase purity and structural data were determined by x-ray and neutron diffraction in combination with a Rietveld refinement of the recorded patterns [9].

Table 1
La_2RuO_5 single crystal refinement parameters.

Sum formula	La_2RuO_5
Molar mass (g/mol)	458.885
Crystal system	Monoclinic
Space group	$P2_1/c$ (No. 14)
Diffractometer	STOE IPDS 2T
Radiation	$Mo-K_\alpha$: $\lambda = 0.71073$ Å
a (Å)	9.1881(12)
b (Å)	5.8311(7)
c (Å)	7.9658(9)
β (°)	100.793(10)
Volume (Å^3)	419.23
Formula units per cell	4
Temperature (K)	293(2)
Calculated density (g/cm^3)	7.27
Crystal size (mm^3)	$0.05 \times 0.05 \times 0.02$
Absorption coefficient (mm^{-1})	23.47
F(000)	792.0
2θ range (°)	$8.72 \le 2\theta \le 79.98$
Range in *hkl*	$\pm 16, \pm 9, \pm 11$
Total no. of reflections	3888
No. of rejected reflections	159
Independent reflections	1428 ($R_{int} = 0.0566$)
Reflections with $I > 4\sigma(I)$	903 ($R_\sigma = 0.0601$)
Data/parameters	1428/74
Absorption correction	Numerical
Goodness-of-fit (F^2)	0.939
Final *R* indices ($I > 4\sigma(I)$)	$R_1 = 0.0386$, $wR_2 = 0.0883$
R indices (all data)	$R_1 = 0.0730$
Largest differ. peak/deepest hole ($e\cdot$ Å^3)	2.11/−2.31

EXAFS measurements were performed at the beamlines E4 (for the L_{III}-edges) and X1 (for the K-edges) of HASYLAB at DESY. The spectra were recorded at room temperature in transmission mode. The samples for the K-edge investigations consisted of roughly 100 mg $La_{2-x}Ln_xRuO_5$ and 20 mg cellulose. These powders were mixed and pressed to pellets of 13 mm diameter. At the lower energies of the L_{III} edges less sample material was needed. Approximately 50 mg $La_{2-x}Ln_xRuO_5$ was glued on adhesive tape, which was assembled in five layers. The used energy ranges and monochromators are listed in Table 5 for the different absorption edges. In the EXAFS region equidistant *k* steps ($\Delta k \approx 0.04$ Å^{-1} at K-edges and $\Delta k \approx 0.05$ Å^{-1} at L_{III}-edges) were used and the integration time was linearly increased with *k*. The Ru-K data was energy calibrated against the first inflection point of the simultaneously recorded spectra of Ru-metal powder. Other reference materials were Mn and Co metal-foil for the Sm-L_{III} and Dy-L_{III} edge, respectively.

To enhance the signal to noise ratio for Pr-K, Nd-K, Sm-L_{III}, Gd-L_{III}, and Dy-L_{III}, the measurements were repeated four times and the spectra were subsequently averaged. For the La-K measurement a single spectrum was sufficient. The k^3-weighted $\chi(k)$ of the La-K-, Nd-K- (top) and the Sm-L_{III}-, Dy-L_{III}-edges (bottom) are depicted in Fig. 1 to show the different experimental data quality. Data evaluation was performed with the program VIPER [16]. All spectra were energy calibrated setting the absorption edge energies to their literature values (Table 5) and normalized. The pre-edge background μ_b was determined by fitting a polynomial function (with coefficients x^{-3} and x^1) to the pre-edge region. The atomic absorption coefficient μ_0 was obtained from a smoothing spline fit of the post-edge region. For the conversion from energy to *k*-space the threshold energy E_0 was calculated from the maximum of the first derivative of the normalized spectra. The finally obtained $\chi(k)$ curves were fitted using the program WinXAS [17]. After weighting with k^2 or respectively k^3

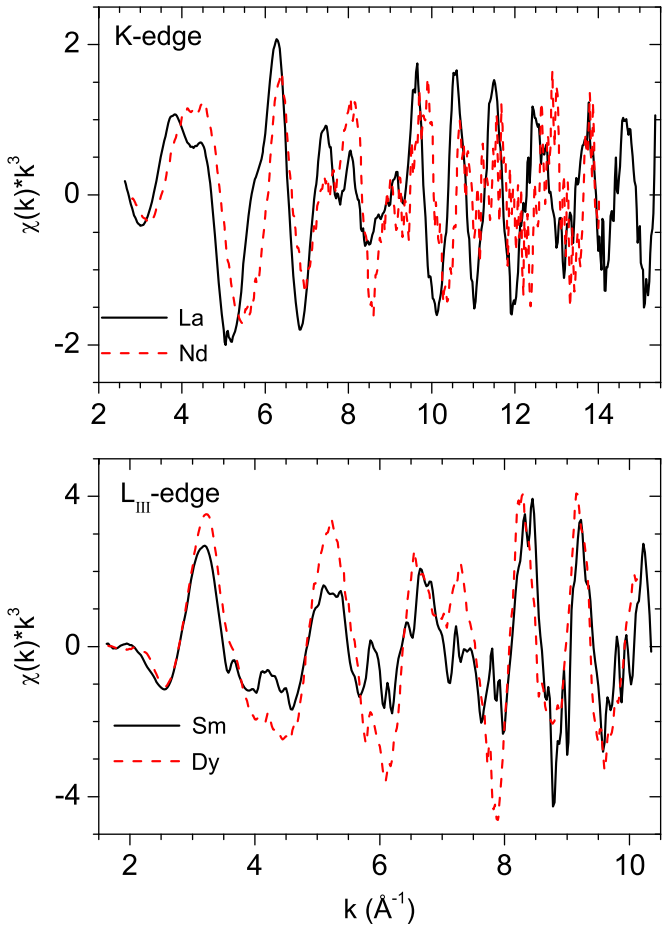

Fig. 1. k^3-weighted EXAFS spectra of the La- and Nd-K- (top) and the Sm- and Dy-L_{III}-edges (bottom) of polycrystalline $La_{2-x}Ln_xRuO_5$ samples.

a Bessel window was applied and the spectra were Fourier transformed resulting in the modified radial distribution functions (mRDFs). Theoretical scattering amplitudes and phase shifts were calculated by FEFF8 using the structure data from the single crystal refinement [18].

3. Results

3.1. Single crystal structure refinement

Several crystals were tested and all turned out to be twins. Nevertheless, a structure analysis was possible due to the partially merohedral nature of the twinning, which allowed the separation of the diffraction patterns of both twin domains. Overlapping peaks were neglected in the refinement. In Table 1 the refinement and crystal parameters are shown. Unit cell values very close to the ones obtained from powder x-ray and neutron diffraction and the same monoclinic space group $P2_1/c$ were found [6,9]. The single crystal analysis leads to similar atomic coordinates (Table 2), therefore, the bonding lengths and angles of the single crystal are comparable to the results from the neutron powder diffraction.

In Fig. 2 the obtained crystal structure is depicted. The ellipsoids represent the anisotropic displacement factors (Table 3) with 90% probability. Alternating LaO and $LaRuO_4$ layers along **a** can be used to describe the crystal structure as was already suggested from powder diffraction data [1]. The $LaRuO_4$ layers consist of perovskite like corner sharing RuO_6 octahedra,

Table 2
Atomic coordinates and isotropic equivalent displacement parameters U_{eq} in Å^2 for the La_2RuO_5 single crystal. U_{eq} is defined as one-third of the trace of the orthogonalised U_{ij} tensor.

Atom	x	y	z	U_{eq}
La1	0.1689(1)	0.2504(1)	0.0387(1)	0.0077(1)
La2	0.5519(1)	0.2628(1)	0.3794(1)	0.0072(1)
Ru	0.8504(1)	0.2540(1)	0.2114(1)	0.0051(1)
O1	0.8544(9)	0.3325(12)	0.4623(6)	0.0090(11)
O2	0.6880(9)	0.4607(12)	0.1300(7)	0.0101(12)
O3	0.7231(10)	−0.0111(12)	0.2213(8)	0.0127(15)
O4	1.0211(11)	0.0441(14)	0.2933(8)	0.0155(15)
O5	0.4237(9)	0.3328(12)	0.6030(7)	0.0093(11)

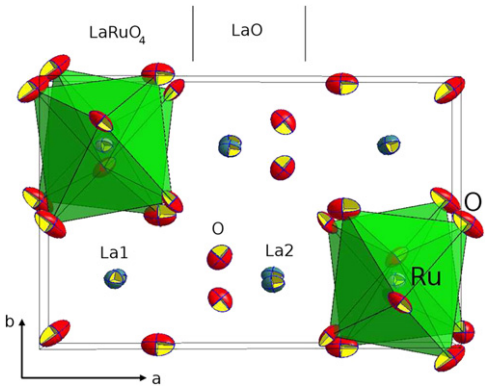

Fig. 2. La_2RuO_5 crystal structure viewed along **c**-direction. La is drawn in dark blue, oxygen in red and Ru in light grey in the center of the green RuO_6 octahedra. The anisotropic displacement ellipsoids are shown with 90% probability. On the top the $LaRuO_4$ and LaO layering is indicated. (For interpretation of the references to color in this figure legend, the reader is referred to the web version of this article.)

Table 3
Anisotropic displacement factors U_{ij} in Å^2 for the La_2RuO_5 single crystal.

Atom	U_{11}	U_{22}	U_{33}
La1	0.0081(2)	0.0066(2)	0.0083(2)
La2	0.0098(2)	0.0062(2)	0.0059(2)
Ru	0.0059(3)	0.0045(2)	0.0052(2)
O1	0.0110(37)	0.0095(29)	0.0073(25)
O2	0.0094(38)	0.0098(31)	0.0102(27)
O3	0.0215(51)	0.0098(32)	0.0086(30)
O4	0.0189(44)	0.0134(37)	0.0123(30)
O5	0.0116(35)	0.0122(30)	0.0041(25)

Atom	U_{23}	U_{13}	U_{12}
La1	0.0005(1)	0.0011(1)	0.0002(2)
La2	−0.0014(2)	0.0023(1)	−0.0003(2)
Ru	0.0004(2)	0.0015(1)	−0.0002(3)
O1	−0.0004(17)	0.0035(17)	0.0046(24)
O2	−0.0031(17)	−0.0008(18)	−0.0046(24)
O3	−0.0014(18)	0.0070(23)	0.0003(28)
O4	−0.0021(20)	−0.0004(21)	0.0089(31)
O5	0.0025(16)	0.0013(17)	0.0025(24)

which are tilted and additionally slightly deformed due to the unequal Ru–O bond lengths listed in Table 4. The perovskite layers are separated by buckled LaO layers with tetrahedral La coordinated oxygen atoms, as depicted in detail in Fig. 3. Each oxygen atom in this layer is connected to one La atom in the $LaRuO_4$ and three in the LaO layer [1]. The tetrahedra are highlighted in the figure by light blue coloring.

Table 4
Selected bond lengths and interatomic distances for the La_2RuO_5 single crystal.

Bond	d (Å)	Bond	d (Å)
Ru–O1	2.044(5)	La1–La1 (× 2)	3.9829(6)
Ru–O1	2.055(5)	La1–La1	4.2149(6)
Ru–O2	1.933(8)	La1–La1	4.2219(6)
Ru–O3	1.949(8)	La1–La2	3.8030(6)
Ru–O4	2.001(8)	La1–La2	3.9123(6)
Ru–O4	2.067(8)	La1–La2	3.9596(6)
		La1–La2	4.0224(6)
Ru–La1	3.4588(8)	La2–La1	3.8030(6)
Ru–La1	3.4957(9)	La2–La1	3.9123(6)
Ru–La1	3.5359(9)	La2–La1	3.9596(6)
Ru–La1	3.5361(9)	La2–La1	4.0224(6)
Ru–La1	3.5388(9)	La2–La2 (× 2)	3.5950(6)
Ru–La1	3.5703(9)	La2–La2	3.5973(6)
Ru–La2	3.2690(8)	La2–La2	3.8321(6)
Ru–La2	3.4364(8)	La2–La2 (× 2)	3.9857(6)

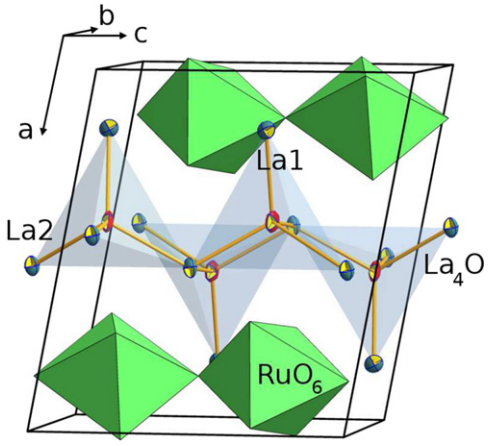

Fig. 3. La_2RuO_5 crystal structure emphasizing the La_4O tetrahedra (light blue). The RuO_6 octahedra are depicted in green. Anisotropic displacement ellipsoids represent a 90% probability. (For interpretation of the references to color in this figure legend, the reader is referred to the web version of this article.)

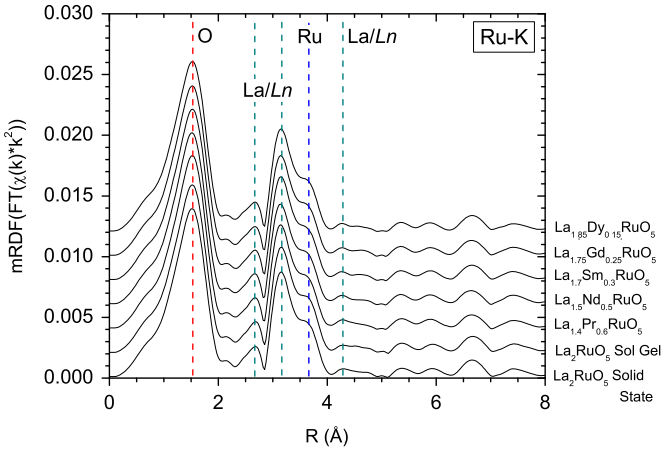

Fig. 4. Modified radial distribution function from the k^2-weighted Ru-K EXAFS spectra. The vertical dashed lines mark the different coordination shells of Ru (curves are shifted by 0.002).

3.2. Ru-K EXAFS

In Fig. 4 the modified radial distribution functions of the Ru-K EXAFS for the $La_{2-x}Ln_xRuO_5$ compounds with a high substitution level for each rare earth element are shown. The corresponding curve for unsubstituted La_2RuO_5 (solid state and sol gel synthesis) is additionally shown for comparison. All EXAFS spectra were weighted by k^2 and oscillations between $k=2$ and 15 $Å^{-1}$ were used for the Fourier transformation.

Up to 4 Å, well defined peaks according to the different coordination spheres can be identified in the mRDF (Fig. 4). The peaks at roughly 1.8, 2.7/3.2, 3.7, and 4.3 Å represent the neighboring O, La/*Ln*, Ru, and a second shell of La/*Ln*, respectively. The peak positions of the unsubstituted La_2RuO_5 are marked with dashed lines for better comparability. Since the Ru–O bonding lengths vary between 1.933 Å and 2.067 Å (Table 4) the peak resulting from the backscattering of the oxygens is broadened and asymmetric. With FEFF8 the amplitudes and phase shifts for the backscattering atoms were modelled and used for fitting the measured data of La_2RuO_5 prepared by the sol gel method. Using the scattering paths for the coordinating atoms up to roughly 5 Å distance, the result is in very good agreement with the experimental data (Fig. 5). In Table 6 the obtained values from the fit are listed. In Ref. [11], Arcon et al. reported an EXAFS fit using a more complex model. We tried this model in a first attempt, but found that reducing the number of fit parameters by combining several backscattering paths with similar interatomic distances lead to a more stable result. During the refinement of the undoped La_2RuO_5 the coordination numbers N were kept fix and the Debye–Waller factors σ^2 were constrained to be equal for the backscattering atoms of the same element in equivalent coordination shells. In a second refinement step S_0^2 and σ^2 were fixed to the values previously obtained and N and the distances were refined. The model was further improved by neglecting all Ru–O paths above approximately 3.5 Å. Their contribution is of minor relevance for the fit and the obtained values in the first attempts were not reliable. Multiple scattering was not taken into account since its contribution was negligible compared to the direct scattering. Multiple scattering occurs for colinear arrangements, i.e. bond angles close to 180° [19], which are not present in $La_{2-x}Ln_xRuO_5$ [6,9]. The Ru–O–Ru bonding angles of ≈155° in the **ab**-plane (respectively ≈153° along **c**) are comparable to the situation in $CaCu_3Ru_4O_{12}$ with Ru–O–Ru ≈140°, in which the multiple scattering could also be neglected [20].

By combining several backscattering shells as described above a reasonable simplification was achieved, which lead to a stable fit. The Ru–O distances were rearranged in two shells, which represent the two shorter bond lengths of O2 and O3, which are pointing to the LaO layers, and the four longer bond lengths of O1 and O4, respectively. The obtained distance of 1.909 Å is slightly

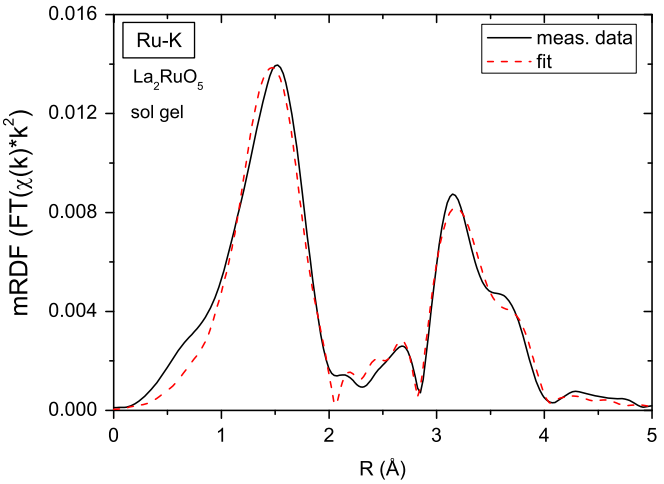

Fig. 5. Fit (dashed line) of the mRDF of the k^2-weighted $\chi(k)$ measured at the Ru-K absorption edge of La_2RuO_5 (solid line) prepared by the sol gel route.

shorter than the values of the single crystal results (see Table 4). On the other hand the second distance representing the four oxygen atoms crosslinking the RuO_6 octahedra in the $LaRuO_4$ layer gave an averaged distance of 2.042 Å, which is in good agreement with the single crystal data (between 2.001 and 2.067 Å, averaged distance 2.041 Å). From the distribution of the distances in Table 4 it can be seen that the eight Ru–La distances can be grouped into four sets with a degeneracy of 1, 4, 2, and 1. Therefore, four scattering shells were used to fit the first two La-related peaks. The obtained distances from the EXAFS spectra are only slightly longer by between 0.01 Å and 0.04 Å than the ones shown in Table 4. For the Ru–Ru backscattering a single shell with a coordination number of four was sufficient, while two different distances were used to model the third Ru–La peak. The obtained EXAFS distances are again distinctly larger by 0.04–0.1 Å than expected from the single crystal data. In general the obtained interatomic distances from EXAFS spectroscopy agree well with the values derived from the diffraction results. The small deviations observed are most likely due to the simplified model applied. The deviations of the coordination numbers from the EXAFS fit to the expected values are small, which proves that the used model is applicable and leads to stable results.

The fitting procedure described above was applied to all spectra and resulted in very similar values. Thus it can be concluded that substitution by rare earth ions does not lead to a considerable distortion of the Ru environment. This corresponds well to the Ru–O bond lengths and angles obtained from x-ray and neutron powder diffraction. Also with these diffraction methods only very small deviations of bond lengths and angles in the RuO_6 octahedra were observed for $La_{2-x}Ln_xRuO_5$ [9].

The XANES (x-ray absorption near edge structure) region of the Ru-K edge was used for the determination of the Ru valence. The first maximum of the derivative of the spectra was taken as energy measure. A comparison showed that all compounds exhibit very similar absorption edge energies. Thus the Ru valence is +4 for all $La_{2-x}Ln_xRuO_5$ compounds in accordance with results on La_2RuO_5 reported by Arcon et al. [11].

3.3. Ln-K EXAFS

The absorption edges of the rare earths were measured to investigate the cationic ordering in the substituted compounds. As described in the Introduction, neutron diffraction revealed a preferred occupation of Pr on the La2 site, i.e. within the LaO-layers [9]. Due to similar neutron scattering lengths of La and the substituting rare earth (e.g. La 8.24 fm, Nd 7.69 fm) and/or high absorption coefficients (e.g. Sm 5922 bn, Gd 49700 bn) this method could not be used for the other lanthanides [21]. Since XAS is highly element specific, it allows the investigation of the surrounding of the substituting elements. In Table 5 the K- and L_{III}-absorption-edge energies of the used lanthanides are listed.

Table 5
Parameters for the EXAFS measurements.

Edge	Energy (keV) [15]	Monochromator	EXAFS range (keV)	Δk (Å^{-1})
La-L_{III}	5.483	Si(111)	5.503–5.895	0.05
La-L_{II}	5.891			
La-L_I	6.266			
Sm-L_{III}	6.716	Si(111)	6.736–7.310	0.055
Gd-L_{III}	7.243	Si(111)	7.263–7.930	0.056
Dy-L_{III}	7.790	Si(111)	7.810–8.585	0.05
Ru-K	22.117	Si(311)	22.160–24.000	0.05
La-K	38.925	Si(511)	38.970–40.000	0.04
Pr-K	41.991	Si(511)	42.030–43.100	0.04
Nd-K	43.569	Si(511)	43.620–44.800	0.04

The L_{III}-edge energies of La, Pr and Nd are too similar in energy to be evaluated separately. Thus the strong overlapping of the EXAFS regions of La and Pr/Nd demands the investigation of the K-edges of these elements. The larger energy difference of the K-edges enables a clear separation of the EXAFS spectra. However, for the late 4f-elements like Sm, Gd and Dy the energy finally becomes so high that the EXAFS oscillations are of very low amplitude, e.g. at the Sm-K edge no significant oscillations were observed. For these elements the L_{III}-edges were therefore investigated as described in Section 3.4.

The fitting of the *Ln*-EXAFS data is complicated by the fact that the rare earths under investigation can occupy both crystallographic La sites, i.e. the one in the $LaRuO_4$-layers and the one in the LaO-layers. Thus the obtained spectra contain contributions from both sites. Looking at the interatomic distances listed in Table 4 it is obvious that for both La positions a large number of different backscattering paths have to be considered. Therefore, certain simplifications were applied to reduce the number of fitting parameters with a conservation of accuracy. First of all, all backscattering rare earth elements were treated as lanthanum. This simplification is justified by almost identical backscattering amplitudes and phases calculated with FEFF8. As a second simplification the La-oxygen coordination sphere was not considered. The oxygen environment is composed of the contributions of many different oxygen ions with strongly varying La–O distances. In addition the coordination numbers are very similar for both La sites. La1 in the $LaRuO_4$ layer is surrounded by 12 oxygen atoms and La2 in the LaO layers has 10 oxygen neighbors. For both sites the distances vary in the range R(La–O) $\approx 2.35-2.98$ Å with a very regular length-distribution. Thus a fit of the oxygen coordination sphere does not help to distinguish the two La sites and was therefore not performed.

From the single crystal structure results it was found that the La1 site in the perovskite like $LaRuO_4$ layers is surrounded by six Ru ions (3.4588 Å $\leq R \leq$ 3.5703 Å). In contrast the La2 site in the LaO layer is well separated from the Ru ions. As a result only two La–Ru distances with shorter lengths of $R=3.2690$ Å and 3.4364 Å need to be considered for this site. In the following the Ru coordination sphere of La2 is denoted as Ru(α) due to the shorter distances and Ru(β) is used for the La1 site. Ru(α) thus consists of two Ru ions with an average distance of 3.35 Å, while Ru(β) contains six Ru ions at an average distance of 3.52 Å. The values of the average distances derived from the single crystal analysis and the variance of the distribution range of distances, which reflects the "thickness" of the coordination shell, are listed in Table 7.

The La/*Ln* coordination of the La1 and La2 sites requires a more detailed discussion. La1 is surrounded by eight La/*Ln* atoms, which can be divided in six shorter distances with values between 3.80 Å and 4.02 Å and two clearly longer distances of $\approx$4.21 Å. In

Table 6
Ru-K EXAFS fit results for polycrystalline La_2RuO_5 obtained by sol gel reaction. With the simplified fit-model described in the text a residual of 13.10% was achieved. The spectra was k^2 weighed, the E_0 shift was −2.58(1) eV and S_0^2 amounted to 0.910(1).

Coordination	*N*	*R* (Å)	σ^2 (Å^2)
Ru–O	1.96(1)	1.909(1)	0.0013(1)
Ru–O	4.01(1)	2.042(1)	0.0013(1)
Ru–La	0.98(1)	3.280(1)	0.0047(1)
Ru–La	3.94(1)	3.477(1)	0.0047(1)
Ru–La	1.98(1)	3.574(1)	0.0047(1)
Ru–La	0.95(1)	3.640(1)	0.0047(1)
Ru–Ru	4.11(1)	4.013(1)	0.0080(1)
Ru–La	0.98(2)	4.694(1)	0.0039(1)
Ru–La	0.90(2)	4.838(1)	0.0039(1)

Table 7
Averaged distances calculated from La_2RuO_5 single crystal data. The values in brackets represent the variance of the coordination shells.

EXAFS path	Atoms	Average distance d (Å)
Ru(α)	La2–Ru	3.35(7)
Ru(β)	La1–Ru	3.52(5)
La(α)	La–La	3.87(15)
La(β)	La1–La1	4.22(2)

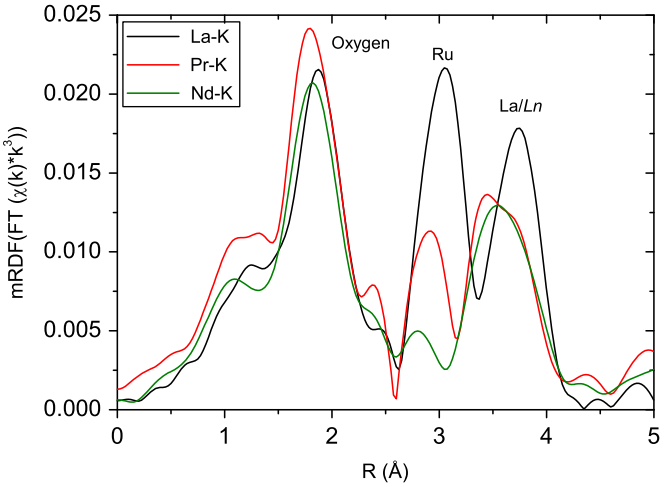

Fig. 6. Fourier transforms (mRDF) of the k^3 weighted EXAFS function $\chi(k)$ of the La-K-, Pr-K- and Nd-K-absorption edge.

contrast, the La2 site has a 10-fold La-coordination with distances between 3.59 Å and 4.02 Å. The coordination spheres are therefore rather similar for both La sites. Although this backscattering shell is thus not very well suited for distinguishing La1 and La2 it had to be included in the fitting procedure due to the overlap of the Ru- and La/*Ln*-shells clearly visible in Fig. 6. To describe these coordination shells the nomenclature La(α) for the 16 shorter bonds and La(β) for the two longer bonds was chosen. The combined backscattering of both La sites contributes in the fitting process of the La-K spectrum. This situation is expected to be different for the *Ln*-K spectra due to the preferred localization described below.

The distribution of the Ln^{3+} ions was derived from the combined fitting of the Ru(α)/Ru(β) and the La(α)/La(β) coordination spheres. If the substituting rare earth *Ln* was occupying solely the La(2) site, the following coordination numbers would result: Ru(α) 2, Ru(β) 0, La(α) 10, and La(β) 0. On the other hand, for a completely random distribution of *Ln* the expected coordination numbers are Ru(α) 2, Ru(β) 6, La(α) 16, and La(β) 2. These numbers are given as N_{theo} (total) and N_{theo} (La2 site) in the second and third line of Tables 8 and 9. Because of these different coordination numbers the intensity ratio of the Ru and La/*Ln* peak are expected to change compared to the La-K-edge spectrum, if a (partial) cation ordering is present. In Fig. 6 the mRDF for the three recorded K-edges are shown in comparison. The peaks are indicating the coordination shells of oxygen at approximately 1.8 Å, Ru at $\approx$3.0 Å and La/*Ln* at $\approx$3.7 Å. For La-K the intensity of the Ru-related peak is larger than the one of the La/*Ln*-shell, while for Pr-K and Nd-K the Ru peak is explicitly smaller than the La/*Ln* peak. This is already a hint for a non-statistical site distribution.

For a quantitative analysis the fitting of the La-K spectra was carried out using the four shell model described above. In this

Table 8
EXAFS refinement results for the K-edge measurements.

Edge	S_0^2	E_0 (eV)		Ru(α)	Ru(β)	La(α)	La(β)
			N_{theo} (total)	2	6	16	2
			N_{theo} (La2 site)	2	0	10	0
La-K (La_2RuO_5)	0.56(1)	−7.28(5)	N	2	6.07(7)	16.29(20)	1.99(3)
		Res = 9.72%	R (Å)	3.245(1)	3.480(1)	3.905(1)	4.234(1)
			σ^2 ($\times10^{-3}$ Å^2)	8.77(7)	8.90(5)	15.88(7)	5.21(6)
Pr-K ($La_{1.4}Pr_{0.6}RuO_5$)	0.34(1)	−8.68(11)	N	2	4.14(6)	13.34(16)	1.58(2)
		Res = 12.46%	R (Å)	3.194(1)	3.439(1)	3.852(1)	4.232(1)
			σ^2 ($\times10^{-3}$ Å^2)	6.90(6)	9.20(4)	10.71(4)	3.13(4)
Nd-K ($La_{1.5}Nd_{0.5}RuO_5$)	0.25(1)	−9.76(21)	N	2	4.68(16)	19.89(38)	2.72(6)
		Res = 7.19%	R (Å)	3.145(1)	3.378(2)	3.846(2)	4.227(2)
			σ^2 ($\times10^{-3}$ Å^2)	6.36(7)	12.67(6)	11.58(10)	3.85(10)

Table 9
EXAFS refinement results for the L_{III}-edge measurements.

Edge	S_0^2	E_0 (eV)		Ru(α)	Ru(β)	La(α)	La(β)
			N_{theo} (total)	2	6	16	2
			N_{theo} (La2 site)	2	0	10	0
Sm-L_{III} ($La_{1.70}Sm_{0.30}RuO_5$)	0.49(1)	6.17(1)	N	2	3.96(1)	14.18(2)	1.44(1)
		Res = 11.64%	R (Å)	3.294(1)	3.394(1)	3.939(1)	4.225(1)
			σ^2 ($\times10^{-3}$ Å^2)	7.37(2)	10.82(2)	13.06(2)	5.43(2)
Gd-L_{III} ($La_{1.75}Gd_{0.25}RuO_5$)	1.17(1)	5.97(3)	N	2	3.91(15)	19.67(17)	2.84(4)
		Res = 11.88%	R (Å)	3.276(2)	3.392(2)	3.925(5)	4.141(11)
			σ^2 ($\times10^{-3}$ Å^2)	14.21(25)	13.98(25)	29.61(31)	8.39(34)
Dy-L_{III} ($La_{1.85}Dy_{0.15}RuO_5$)	0.68(1)	5.59(1)	N	2	4.60(2)	11.65(2)	1.45(1)
		Res = 17.28%	R (Å)	3.257(1)	3.373(1)	3.983(1)	4.304(1)
			σ^2 ($\times10^{-3}$ Å^2)	7.23(3)	7.48(3)	14.13(3)	4.10(3)

model the scattering paths of Ru and La/*Ln* ions with similar distances are unified to a single backscattering shell with an averaged interatomic distance. This procedure is commonly used to reduce large numbers of scattering amplitudes and phases. For example for the compound $Ce_{1-x}La_xO_{2-x/2}$ averaged coordination spheres of O and La/Ce were used to fit the EXAFS spectra in a similar procedure [22].

The fit applying this four shell model for the unsubstituted La_2RuO_5 is depicted in Fig. 7. The calculated and measured mRDF match very well in the fitting region (2.5–4.2 Å). The contributions of the four shells are shown as solid lines (shifted for clarity) and the summation is depicted as dashed line.

In Table 8 the results of the fitting parameters for the La-K, Pr-K and Nd-K spectra are listed. In the first step of the fitting procedure the amplitude reduction factor S_0^2 and the energy shift E_0 of the La-K spectra were refined while averaged values of the distance (R) taken from single crystal data and the Debye–Waller factors (σ^2) were kept fixed. In addition the theoretical values N_{theo} (total) were used as coordination numbers. The same shift of the threshold energy E_0 was used for all backscattering shells. In a next step R and σ^2 were refined with fixed E_0 and N. Finally only the coordination numbers and S_0^2 were refined resulting in the values shown in Table 8. In all runs the coordination number N(Ru(α)) was fixed to 2 in order to enhance the stability of the refinement and because this value is the same for both a statistical and a completely ordered distribution of *Ln*.

The obtained residuals [20] (Res) given in Table 8 indicate a good fit quality. The rather high values for Debye–Waller factors of Ru(β) (12.67×10^{-3} Å^2 for Nd-K) and La(α) (15.88×10^{-3} Å^2 for La-K) result from the large spreading of the interatomic distances unified to one backscattering shell in the fit. The σ^2 of the remaining two paths is significantly smaller (roughly 7×10^{-3} Å^2 for Ru(α) and respectively 3×10^{-3} Å^2 for La(β)), because only two quite similar distances were averaged here.

For the La-K edge of La_2RuO_5 the obtained coordination numbers agree well with the expected values and prove that the simplified model (Table 8) can in fact be used for data analysis. This is illustrated in Fig. 7, where the resulting sum matches the experimental mRDF very well. The obtained distances of the backscattering shells are in very good agreement with the merged values listed in Table 7. Only the distance for Ru(α) was approximately 0.1 Å shorter than expected from the single crystal analysis.

The same fitting procedure was used for the Pr-K and Nd-K spectra, leading to the values listed in Table 8. The obtained distances are distinctly smaller than the values calculated from the single crystal data listed in Table 7. These shorter interatomic distances correspond well with the observed decrease of the unit cell parameters upon rare earth substitution (see Ref. [9]). The obtained values are quite similar for $La_{1.4}Pr_{0.6}RuO_5$ and $La_{1.5}Nd_{0.5}RuO_5$ (in detail the distances are slightly smaller for the latter one), which agrees with the similar unit cell parameters for both compounds [9].

Comparing the coordination numbers for the Pr-K and Nd-K edge spectra, it can be seen that the obtained number of backscattering atoms in the Ru(β) shell is clearly smaller than expected for a random distribution of Nd or Pr on the two La sites. For the La(α) and La(β) shells the differences of the coordination numbers are less reliable mostly due to the quality of the absorbtion spectra, which became rather noisy at high k-values because of the high absorption of lanthanum. In fact coordination numbers even larger than expected for a statistical distribution were in some cases observed (see Table 8). These may of course be avoided by appropriate constrains, which we did not apply to avoid biases in the results. We found N(Ru(β)) to be the most reliable measure for the distribution of the substituting rare earths and values of 4.14 for Pr and 4.68 for Nd correspond to 65% and 61% of the substituting rare earth on the La2 site. This is in very good accordance with the 65–70% for Pr derived from neutron diffraction [9].

3.4. *Ln-L$_{III}$ EXAFS*

The EXAFS spectra of the *Ln*-K-edge of Sm, Gd and Dy did not exhibit evaluable oscillations, therefore we used the L_{III}-edges of these elements. The Sm-L_{III} absorption edge has a sufficiently higher energy than the La-L_I edge (Table 5). Gd and Dy possess even higher L_{III}-edge energies, thus an overlapping with the La-L_I-edge does not need to be considered.

The spectra were recorded and evaluated similar to the procedure described above for *Ln*-K-edges. The mRDFs of the rare earth L_{III}-edge spectra are depicted in Fig. 8. It is noteworthy that the signal-to-noise ratio at the L_{III}-edges of Sm, Gd, and Dy was by far worse that for the K-edge spectra of Pr and Nd (see Fig. 1). Due to the smaller maximum substitution levels for the late rare earths (e.g. $x_{max} = 0.2$ for Dy in comparison to $x_{max} = 0.75$ for Pr) rather small $\Delta(\mu)$ values were observed at the L_{III}-edges. Because of the high absorption of the compounds, the thickness of the

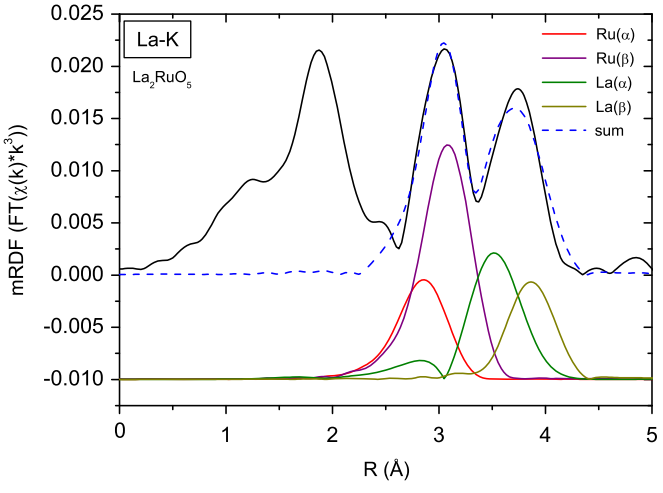

Fig. 7. Fit results for the La-K mRDF. Ru(α), Ru(β) and La(α), La(β) indicate scattering paths for the two different crystallographic La sites (see text for details).

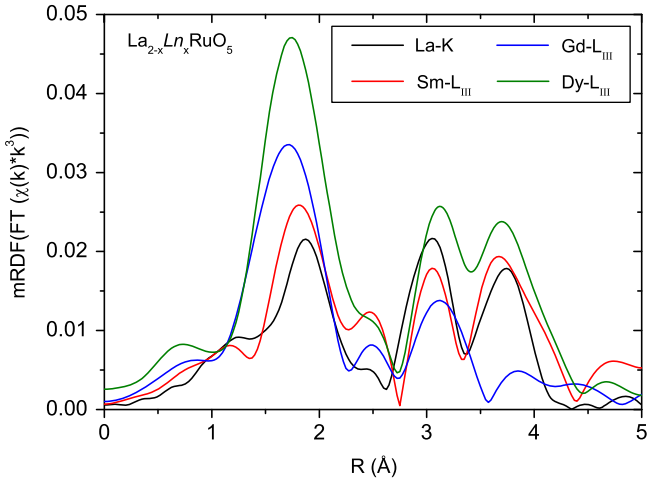

Fig. 8. Fourier transforms (mRDF) of $\chi(k) \cdot k^3$ at the *Ln*-L_{III}-absorption edges of $La_{2-x}Ln_xRuO_5$. The corresponding mRDF from the La-K EXAFS is shown for comparison.

samples had to be small. For these reasons, only edge jumps of $\Delta(\mu) \leq 0.1$ could be achieved. As a consequence the useful k range was limited to roughly 7 $Å^{-1}$ (Gd) or 10 $Å^{-1}$ (Sm, Dy). Among the mRDF of the rare earth substituted compounds the curve for Gd shows the smallest peak for the La/*Ln* coordination shells due to the comparable low quality of the measured spectra and the smallest k-range, which was evaluable. Additionally, the small k-region results in an overall broadening of the peaks in the L_{III} mRDFs [10].

Calculation of the scattering amplitudes and phases at the L_{III}-edges was again performed with FEFF8. Similar scattering paths were combined and the same four coordination spheres introduced for the K-edge were used for the fit. A similar simplification was previously described, e.g. for investigations of the L_{III}-edge of Ln_2O_3 [23,24].

For the edge energy correction E_0, the intense white lines at the L_{III}-edges cause an increased shift. The fit of the data was done according to the above described procedure for the K-edges. First the distances R and the energy shifts were refined and in a second step the weighting of scattering paths was refined leaving R and $N(\mathrm{Ru}(\alpha))=2$ fixed.

The fit results are listed in Table 9 for $La_{1.70}Sm_{0.30}RuO_5$, $La_{1.75}Gd_{0.25}RuO_5$ and $La_{1.85}Dy_{0.15}RuO_5$. As was expected for the overall smaller k-range, the Debye–Waller factors of all four backscattering shells are slightly increased compared to the K-edge.

The obtained coordination shell distances agree well with the merged values in Table 7. For Ru(α) the accordance is excellent with approximately 3.3 Å, for Ru(β) the distances of roughly 3.4 Å are slightly shorter than the expected 3.52 Å, while the La backscattering shells show an increased distance compared to the merged values. With increasing distance the deviation between the expected and observed values increases. Taking into account the above described quality of the data such deviations are not surprising.

The obtained coordination numbers show a decrease for $N(\mathrm{Ru}(\beta))$, which is very similar to the one for the Pr and Nd substituted samples. The preferred occupation of *Ln* on the La2 site in the LaO layers is therefore clearly supported by the EXAFS results. The reduction from $N=6$ to 3.96 for Sm, 3.91 for Gd and 4.60 for Dy corresponds to roughly 68%, 69%, and respectively 57% of the *Ln*-ions occupying the La2 site. Again, these findings are in very good agreement with the neutron diffraction result for the Pr-substituted compounds (65–70% of the Pr ions in the LaO layer) [9]. Only for Dy no clear site preference was found in our EXAFS analysis.

4. Conclusions

The structural data obtained from the La_2RuO_5 single crystal refinement agree very well with earlier powder x-ray and powder neutron diffraction results. This proves that the twinning of the crystals and the resulting limitation of the data set (overlapping reflections were neglected) as well as the absorption correction do not comprise the single crystal structure analysis. The crystal structure was used as starting point for local structural investigations of La_2RuO_5 and rare earth substituted $La_{2-x}Ln_xRuO_5$ powder samples by x-ray absorption spectroscopy.

Details of the local surroundings of Ru, La and the rare earths (Pr, Nd, Sm, Gd, Dy) were studied. The Ru-K-edge EXAFS exhibited almost identical coordination of Ru independent of a partial replacement of La by other rare earth ions. A fit of the Ru coordination spheres was successfully carried out using a by far less complicated model compared to an earlier study [11]. With this model interatomic distances were refined and found to agree well with the expected values derived from single crystal x-ray diffraction.

The distribution of the substituting rare earths was determined by EXAFS at the K- or L_{III}-edges, respectively. The data evaluation is complicated by the fact that two crystallographic sites for La/*Ln* are available and thus in the obtained modified radial distribution functions the contributions of both sites overlap. Therefore, a simplified model with a reduced number of coordination shells using averaged interatomic distances was successfully introduced. This model allows to perform the fitting procedure with a reasonable number of free parameters and was applied to the K- and L_{III}-edge EXAFS spectra of $La_{2-x}Ln_xRuO_5$.

The obtained results from the La, Pr and Nd K-edge spectra show a very good agreement with the averaged distances of the four backscattering shells calculated from the single crystal data. The corresponding values for the Sm, Gd and Dy L_{III}-edge spectra showed increasing deviations with increasing distance to the central absorber due to the limited k-range evaluable for the Fourier-transformation.

The rare earth ion distribution was examined by comparing the coordination numbers of the Ru(β) backscattering path. For a random arrangement the coordination number 6 is expected, while a complete cationic ordering with the rare earths solely occupying the La2 site should result in a value of 0. For both the K-edge and the L_{III}-edge spectra coordination numbers of roughly 4 were found. This reduction of $N(\mathrm{Ru}(\beta))$ clearly supports the preferred occupation of the La2 site by the substituting ions and corresponds to roughly 2/3 of the *Ln*-ions on the La2 site and 1/3 on the La1 site. It is noteworthy that the same degree of cationic ordering was found for all lanthanide ions (except for Dy, for which no clear ordering was found). This finding indicates that the size of the ions plays only a minor role for the ordering. The (partial) ordering is in agreement with geometric considerations since the size of the La2 position is smaller than the one of the La1 site and therefore it should be favored by the smaller lanthanide ions. Our results are further supported by earlier neutron powder diffraction studies on selected Pr-substituted samples, which also revealed a cationic ordering of roughly 65–70% of the *Ln*-ions on the La2 site [9].

In summary, our investigations show that important structural information can be obtained from EXAFS spectroscopy especially when diffraction techniques fail. Such structural details can even be derived for low-symmetric compounds like La_2RuO_5, in which the coordination spheres are highly distorted.

Acknowledgments

The authors gratefully acknowledge the financial support of the DFG (SFB 484). Thanks are due to HASYLAB for the allocated beamtime.

References

[1] P. Boullay, D. Mercurio, A. Bencan, A. Meden, G. Drazic, M. Kosec, J. Solid State Chem. 170 (2003) 294–302.
[2] P. Khalifah, R. Osborn, Q. Huang, H.W. Zandbergen, R. Jin, Y. Liu, D. Mandrus, R.J. Cava, Science 297 (2002) 2237–2240.
[3] S.K. Malik, D.C. Kundaliya, R.D. Kale, Solid State Commun. 135 (2005) 166–169.
[4] V. Eyert, S.G. Ebbinghaus, T. Kopp, Phys. Rev. Lett. 96 (2006) 256401.
[5] V. Eyert, S.G. Ebbinghaus, Prog. Solid State Chem. 35 (2007) 433–439.
[6] S.G. Ebbinghaus, Acta Crystallogr. C 61 (2005) i96–i98.
[7] H. Wu, Z. Hu, T. Burnus, J.D. Denlinger, P.G. Khalifah, D.G. Mandrus, L.-Y. Jang, H.H. Hsieh, A. Tanaka, K.S. Liang, J.W. Allen, R.J. Cava, D.I. Khomskii, L.H. Tjeng, Phys. Rev. Lett. 96 (2006) 256402.
[8] S.G. Ebbinghaus, S. Riegg, T. Götzfried, A. Reller, Eur. Phys. J. Spec. Top. 180 (2010) 91–116.

[9] S. Riegg, U. Sazama, M. Fröba, A. Reller, S.G. Ebbinghaus, Phys. Rev. B 84 (2011) 014403.
[10] D.C. Koningsberger, R. Prins, X-Ray Absorption, John Wiley and Sons, New York, 1988.
[11] I. Arcon, A. Bencan, A. Kodre, M. Kosec, X-Ray Spectrosc. 36 (2007) 301–304.
[12] L.H. Brixner, E.P. Moore, Acta Crystallogr. C 39 (1983) 1316.
[13] W. Herrendorf, H. Bärnighausen, *HABITUS*, Program for the Optimization of the Shape of Single Crystals for Numerical Absorption Correction in the Suite *X-SHAPE*, University of Karlsruhe, Karlsruhe, Germany, 1997.
[14] G.M. Sheldrick, *SHELXS-97 and SHELXL-97* Program Suite for the Solution and Refinement of Crystal Structures, University of Göttingen, Göttingen, Germany, 1997.
[15] J.A. Bearden, A.F. Burr, Rev. Mod. Phys. 39 (1967) 125–142.
[16] K.V. Klementiev, J. Phys. D: Appl. Phys. 34 (2001) 209–217.
[17] T. Ressler, J. Synch. Radiat. 5 (1998) 118–122.
[18] A.L. Ankudinov, B. Ravel, J.J. Rehr, S.D. Conradson, Phys. Rev. B 58 (1998) 7565–7576.
[19] S. Ebbinghaus, M. Fröba, A. Reller, J. Phys. Chem. B 101 (1997) 9909–9915.
[20] S.G. Ebbinghaus, A. Weidenkaff, R.J. Cava, J. Solid State Chem. 167 (2002) 126–136.
[21] V.F. Sears, Neutron News 3 (1992) 26–37.
[22] F. Deganello, A. Longo, A. Martorana, J. Solid State Chem. 175 (2003) 289–298.
[23] F. Ali, A.V. Chadwick, M.E. Smith, J. Mater. Chem. 7 (2) (1997) 285–291.
[24] P. Malet, M.J. Capitan, M.A. Centeno, J.A. Odriozola, I. Carrizosa, J. Chem. Soc. Faraday Trans. 90 (18) (1994) 2783–2790.